

# Mechanism of Copper(II) Inhibiting Alzheimer's Amyloid $\beta$ -Peptide from Aggregation: A Molecular Dynamics Investigation

Yong Jiao and Pin Yang\*

Key Laboratory of Chemical Biology and Molecular Engineering of Ministry of Education,  
Institute of Molecular Science, Shanxi University, Taiyuan 030006, China

Received: November 7, 2006; In Final Form: May 5, 2007

The aggregation of an amyloid  $\beta$  peptide ( $A\beta$ ) into fibrils is a key pathological event in Alzheimer's disease (AD). Under certain conditions,  $Cu^{2+}$  markedly inhibits  $A\beta$  from aggregation and is considered as a potential factor in the normal brain preventing  $A\beta$  from aggregation. The possible mechanism of the inhibitory effect of  $Cu^{2+}$  was investigated for the first time by molecular dynamics (MD) simulations. On the basis of the radial distribution function analysis of the MD data, a novel strategy, the  $Q$  function, was proposed to explore the binding sites of  $Cu^{2+}$  by evaluating the coordination priority of atoms in  $A\beta$ , and the [6-5-5] tri-ring 4N binding mode of the  $Cu^{2+}$ - $A\beta$  complexes was found. The mechanism of the conformational transition of  $A\beta$  from the  $\beta$  conformation to distorted  $\beta$  conformations, which destabilizes the aggregation of  $A\beta$  into fibrils, was also revealed. All the results provide helpful clues for an improved understanding of the role of  $Cu^{2+}$  in the pathogenesis of AD and contribute to the development of an anti-amyloid therapeutic strategy.

## 1. Introduction

Alzheimer's disease (AD), the most common neurodegenerative disorder, is characterized pathologically by the presence of extracellular senile plaques and intracellular neurofibrillary tangles in the brain.<sup>1,2</sup> The main constituents of the plaques are amyloid  $\beta$  peptides ( $A\beta$ s) consisting of 39–43 residues that are proteolytically derived from the ubiquitously expressed transmembrane amyloid precursor glycoprotein.<sup>3–6</sup> Compelling evidence suggests that the aggregation of  $A\beta$  is a key event in AD pathology and that neocortical metal ions, especially zinc, copper, and iron ions, may play important roles in the aggregation and toxicity of  $A\beta$  in AD.<sup>6–9</sup> These metals are found in relatively high concentrations in the neocortical regions of the brain most susceptible to neurodegeneration. Microparticle-induced X-ray emission and X-ray fluorescence microscopy studies have revealed that  $A\beta$  amyloid plaques in post-mortem AD brains have an abnormal enrichment of  $Zn^{2+}$ ,  $Cu^{2+}$ , and  $Fe^{3+}$ .<sup>7,8</sup> During neurotransmission, a high concentration of  $Zn^{2+}$  (300  $\mu$ M) is released, which may explain why the precipitation of  $A\beta$  commences in the synapse.<sup>9</sup>

At low micromolar concentrations,  $Zn^{2+}$  rapidly precipitates soluble  $A\beta$  into amyloid aggregates *in vitro*.<sup>10,11</sup> Different from  $Zn^{2+}$  in a wide pH range (>6.0),  $Cu^{2+}$  induces  $A\beta$  aggregating only at mildly acidic pH, which represents physiological acidosis, and yet strongly inhibits  $A\beta$  from aggregation at neutral and basic pH.<sup>12,13,15</sup> Furthermore,  $Cu^{2+}$  competes with  $Zn^{2+}$  and inhibits the  $Zn^{2+}$ -induced aggregation of  $A\beta$ .<sup>14</sup>  $Cu^{2+}$  appeals to many researchers for its potential for being an inhibitor of the aggregation of  $A\beta$  *in vivo*.<sup>13–15</sup> It is reported that in severely degenerated brain regions of AD patients, such as the amygdala and hippocampus, the concentration of  $Cu^{2+}$  is significantly decreased as compared to age-matched controls; however,  $Zn^{2+}$  still remains at comparatively high concentrations.<sup>16</sup> These observations suggest that the effective inhibition of  $Cu^{2+}$  on

the  $Zn^{2+}$ -induced aggregation of  $A\beta$  may be severely weakened by the decrease of  $Cu^{2+}$  concentrations and result in the excessive deposition of  $A\beta$  and the degeneration of the brain.

Although effects of metal ions on the aggregation of  $A\beta$  have been intensely studied, the mechanism of  $Cu^{2+}$  inhibiting  $A\beta$  from aggregation remains to be clarified. There still exists in the literature conflicting statements about the role of  $Cu^{2+}$  in  $A\beta$  plaque formation, and the coordination mode of  $Cu^{2+}$  with  $A\beta$  is awaiting a firm answer. This state of affairs inspired us to perform this work. Computational simulation with atomic level representation has been increasingly used in understanding the complex conformational features of polypeptides and in predicting structural preferences.<sup>17–21</sup> Simulations have been performed by other groups with a view to elucidate the conformational transition and assembly mechanism of  $A\beta$ .<sup>18–21</sup> Herein, the mechanism of  $Cu^{2+}$  inhibiting  $A\beta$  from aggregating was investigated for the first time by molecular dynamics (MD) simulations. On the basis of MD simulations and the radial distribution function analysis of MD data, we propose a novel  $Q$  function to explore the binding sites of  $Cu^{2+}$  by evaluating the coordination priority of atoms in  $A\beta$  and found the coordinating mode of  $Cu^{2+}$  with  $A\beta$ , the [6-5-5] tri-ring 4N mode. Driven by the cooperation of the coordination bonds and their induced intramolecular hydrogen bonds, the conformation of  $A\beta$  transforms from the initial  $\beta$  conformation to distorted  $\beta$  conformations, which destabilizes the aggregation of  $A\beta$ . This work will provide helpful clues for an improved understanding of the role of  $Cu^{2+}$  in the pathogenesis of AD and contribute to the development of an anti-amyloid therapeutic strategy.

## 2. Model and Simulation Methods

### 2.1. Choosing $A\beta$ 10–21 as the Model of Full-Length $A\beta$ .

The structure of  $A\beta$  fibrils lays the foundation for understanding the effects of metal ions on the aggregation of  $A\beta$ . Lynn et al. proposed a three-dimensional structure model of  $A\beta$ 10–35 fibrils, which is characterized by the cross- $\beta$  structure consisting of a lamination of six parallel  $\beta$  sheets propagating along the

\* Corresponding author. Phone/fax: +86-351-7011022; e-mail: yangpin@sxu.edu.cn.

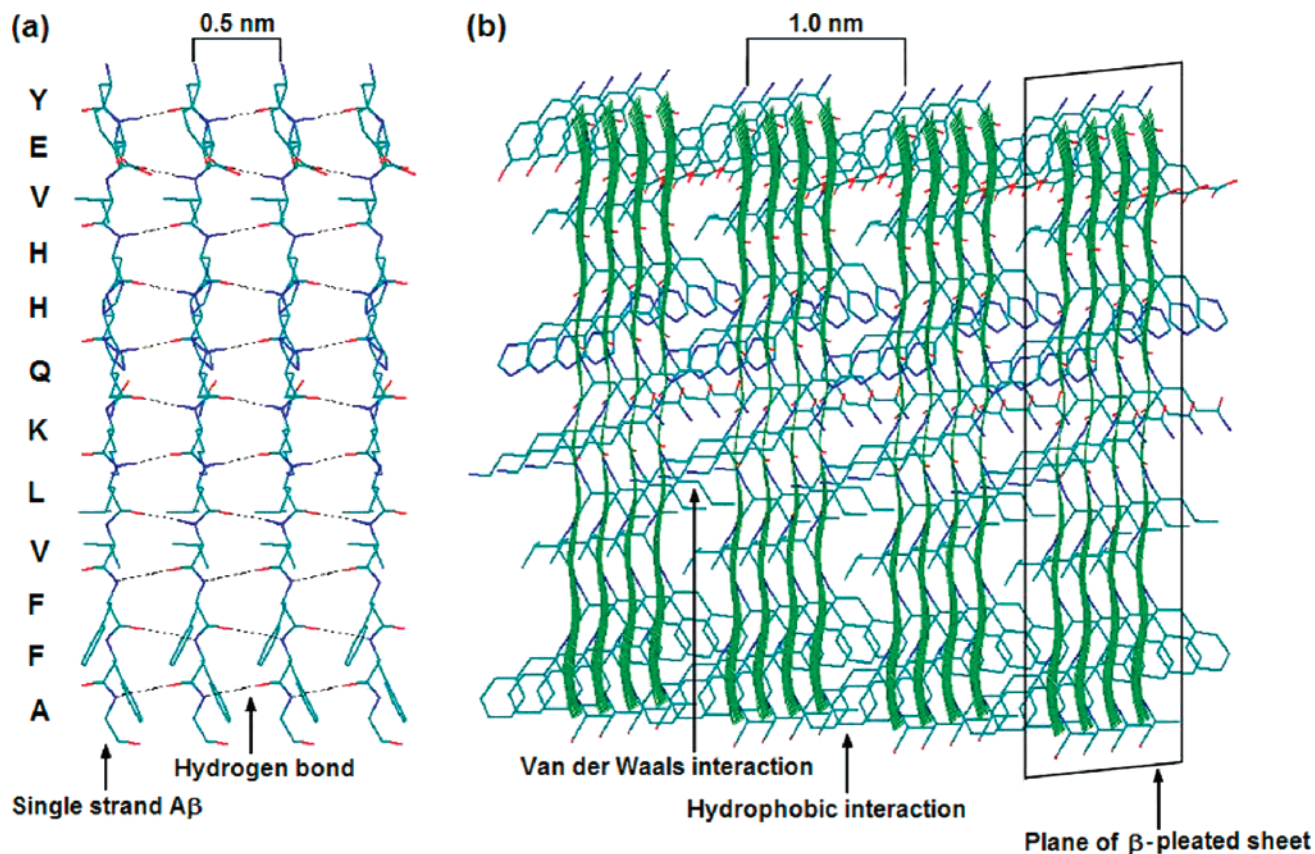


**Figure 1.** Structural model of A $\beta$  fibrils. (a)  $\beta$ -Sheet of four strands spaced in 0.5 nm. (b) Filament of four  $\beta$ -sheets spaced in 1.0 nm.

fibril axis.<sup>22</sup> Within the  $\beta$  sheet, the peptide strands orient themselves perpendicular to the fibril axis. The strands are roughly 0.5 nm apart within the  $\beta$  sheet, and the  $\beta$  sheets have roughly a 1.0 nm separation between each other within the fibrils. Lynn et al. predicted the potential metal binding sites in the fibril by their model.<sup>23,24</sup> Recently, Tycko et al. proposed a structure model of A $\beta$ 1–40 fibrils based on the constraints from solid state NMR data.<sup>25</sup> In Tycko's model, each molecule contained two  $\beta$  strands (residues 12–24 and 30–40), and the oppositely charged side chains of D23 and K28 formed salt bridges.

On the basis of the previous two models and the following considerations, the segment, A $\beta$ 10–21(Y<sup>10</sup>EVHHQKLVFFA<sup>21</sup>), was selected as the model of full-length A $\beta$  in this work. (i) According to Tycko's model,<sup>25</sup> N-terminal residues 1–8 are structurally disordered, and residues 22–29 are in a loop conformation under the influence of the D23–K28 salt bridge. Residues 30–40 form a hydrophobic segment that is not the main segment for metal binding.<sup>13</sup> Those mentioned residues were omitted for lacking a  $\beta$  pleated conformation or metal binding sites, which are essential for metal ion-induced aggregation of A $\beta$ . (ii) It is only the A $\beta$ 10–21 segment that has the same structural characters in the previous two fibril models (i.e., the highly ordered cross  $\beta$  structure assembled by  $\beta$  strands in parallel and in register).<sup>22,25</sup> Especially, A $\beta$ 10–21 contains the histidine dyad, H13, and H14, which play a crucial role in Zn<sup>2+</sup>-induced aggregation of A $\beta$  by forming an H13–Zn<sup>2+</sup>–H14 bridge between the two A $\beta$  strands.<sup>13,23,24</sup> (iii) Experimental and theoretical studies have indicated that A $\beta$ 10–21 is one of the ideal models for investigating the effects of metal ions on the aggregation of A $\beta$ . Lynn et al. found that Zn<sup>2+</sup> induced A $\beta$ 10–21 to aggregate rapidly into typical amyloid fibrils.<sup>24,26</sup> Our study indicates that the mode of Zn<sup>2+</sup> inducing the aggregation of

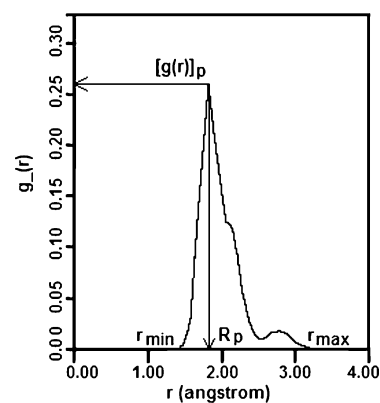


**Figure 2.** Definition of the correlative variables of the  $Q$  function.

A $\beta$ 10–21 is to cross-link the two adjacent A $\beta$ 10–21 strands by a His13(N $\tau$ )–Zn<sup>2+</sup>–His14(N $\tau$ ) bridge,<sup>23</sup> which is consistent with other's results.<sup>13,24,26</sup> Recently, we found that Zn<sup>2+</sup>-induced aggregates of A $\beta$ 10–21 potentiate its action on outward potassium currents in hippocampal neurons, which indicates that Zn<sup>2+</sup>-induced aggregates of A $\beta$ 10–21 are neurotoxic and that A $\beta$ 10–21 may be one of the neurotoxic species of A $\beta$  in vivo, especially if an additional insult, such as Zn<sup>2+</sup>, is present.<sup>27</sup>

**2.2. Simulation Systems.** The focus of this work is on the coordination mode of Cu<sup>2+</sup> with single A $\beta$ 10–21 in solution and the conformational transition effect of Cu<sup>2+</sup> on A $\beta$ 10–21. The Cu<sup>2+</sup>–A $\beta$ 10–21 complex is the primary model system, which consists of a Cu<sup>2+</sup> ion, single A $\beta$ 10–21, and water molecules. The starting structure of A $\beta$ 10–21 with a  $\beta$  conformation is generated within the constraints of Tycko's solid state NMR data by the biopolymer module of the Insight II 2000 program package.<sup>25</sup>

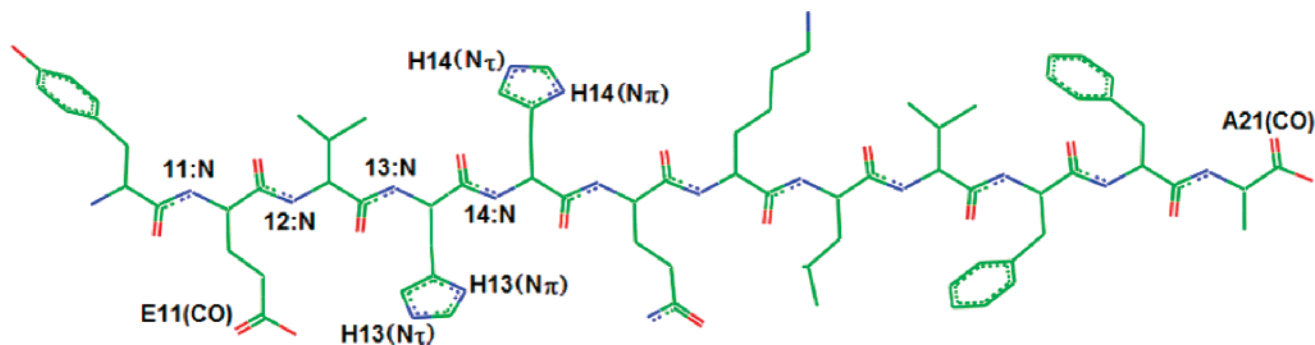


**Figure 3.** Anchor sites and some binding sites of  $\text{Cu}^{2+}$  in  $\text{A}\beta$ .

**TABLE 1. Optimizations of Full Substituted  $\text{Cu}^{2+}$ - $\text{A}\beta$  Complexes with Different Anchor Atoms (kJ/mol)**

residues	anchor sites	energy of complexes
H13	$\text{N}\pi$	-418.9749
	$\text{N}\tau$	-326.0180
H14	$\text{N}\pi$	-366.3477
	$\text{N}\tau$	-308.5765

In our previous work, the multistrand  $\text{A}\beta_{10-21}$  (denoted as  $\text{A}\beta$  next) fibril had been constructed for studying the stabilization effect of  $\text{Zn}^{2+}$  on aggregates.<sup>23</sup> In the section 3.3., we discuss the 16 strand  $\text{Cu}^{2+}$ - $\text{A}\beta$  complex fibril by using the distorted  $\beta$  conformational  $\text{Cu}^{2+}$ - $\text{A}\beta$  complex (the details are discussed in section 3.2.) as the monomer. In contrast, the 16 strand  $\text{A}\beta_{10-21}$  fibril was constructed by using the  $\beta$  conformational  $\text{A}\beta$  as the monomer. First, four strands of  $\text{A}\beta$  with a spacing of 0.5 nm between each other were aggregated to form a  $\beta$  sheet by hydrogen bonds between the main chains of  $\text{A}\beta$ ; then, the four same  $\beta$  sheets with a spacing of 1.0 nm were laminated in parallel to form the cuboid filament (Figure 1). The aim of building the two kinds of fibrils is to preliminarily examine the influence of different conformations of  $\text{A}\beta$  on the

stability of the aggregates by minimizing the fibrils and comparing the system energies.

**2.3. MD Simulations.** The  $\text{Cu}^{2+}$ - $\text{A}\beta$  complexes were simulated in  $35 \text{ \AA} \times 30 \text{ \AA} \times 30 \text{ \AA}$  boxes, except for the first substitution complex in a  $55 \text{ \AA} \times 30 \text{ \AA} \times 30 \text{ \AA}^3$  box. Then, the box was solvated with a simple point charge water model. The resulting system was submitted to energy minimization to remove unfavorable contacts. MD simulations were performed by using the Discover 3.0 package with the canonical ensemble and periodic boundary conditions. All atoms of the system were considered explicitly, and their interactions were computed by using the ESFF force field.<sup>28</sup> The cutoff distance used for the nonbonded interactions was 10  $\text{\AA}$ . All simulations were performed at 310 K, which corresponded to the temperature often used to incubate the amyloid in experiments and near the physiological temperature of humans. For each MD simulation, the integration step was 1 fs. The equilibration time for each of the  $\text{Cu}^{2+}$ - $\text{A}\beta$  complexes was 1 ns followed by 1 ns of data collection for analysis. The radial distribution functions were evaluated by using the Insight II 2000/Analysis module. All calculations was performed on an O2 workstation (Silicon Graphics) with the Insight II 2000 software platform.

**TABLE 2. RDF Evaluation of Coordination Priority of Atoms in [6-5-5]<sup>1</sup> Binding Mode**

substitution order	coordination shell		RDF analysis <sup>a</sup>					
	coordinated atoms	preferential atoms	$[g(r)]_p$	$R_p$	$r_{\min}$	$r_{\max}$	$Q'$ values <sup>b</sup>	$Q$ values
first	H13( $\text{N}\pi$ )		0.28651	2.0	1.9	2.1	0.95177	
		13:N	0.02423	2.7	2.5	4.1		
second	H13( $\text{N}\pi$ )	12:N	0.30028	2.0	1.9	2.1	0.99751	0.87930
			0.03309	2.8	2.6	4.4		
third	H13( $\text{N}\pi$ )	11:N	0.28017	1.9	1.8	2.0	0.97969	
			0.30013	2.0	1.9	2.1		
fourth	H13( $\text{N}\pi$ )		0.02174	2.8	2.6	4.5	0.55707	
		12:N	0.25389	1.9	1.8	2.0		
		13:N	0.30229	1.9	1.8	2.0		
		11:N	0.29140	2.0	1.9	2.1		
		12:N	0.28610	2.0	1.9	2.1		
fifth <sup>c</sup>	H13( $\text{N}\pi$ )	12:N	0.27871	1.8	1.7	1.9	0.92873	
		13:N	0.27854	1.9	1.8	2.0		
		E11(CO)	0.03960	2.6	2.2	3.4		
			0.30802	2.0	1.9	2.1		
		11:N	0.29462	2.0	1.9	2.1		
sixth <sup>c</sup>	H13( $\text{N}\pi$ )	12:N	0.23986	1.9	1.8	2.0	0.83873	
		13:N	0.28456	1.9	1.8	2.0		
		E11(CO)	0.27658	2.2	2.1	2.3		
		A21(CO)	0.08030	2.5	2.0	6.6		
			0.31260	2.0	1.9	2.1		
		11:N	0.30658	2.0	1.9	2.1		
	H13( $\text{N}\pi$ )	12:N	0.27509	1.8	1.8	2.0	1.03843	
		13:N	0.29297	1.9	1.8	2.0		
		E11(CO)	0.26556	2.6	2.5	2.8		
		A21(CO)	0.26150	2.6	2.5	2.8		

<sup>a</sup> On the basis of the conformational space consisting of one million conformers. <sup>b</sup>  $Q'$  values of coordinated atoms (Supporting Information eq S1). <sup>c</sup> Coordination interactions in an axial direction rather than explicitly substituting water molecules.

### 3. Results and Discussion

**3.1. Coordination Mode of Cu<sup>2+</sup>-A $\beta$  Complexes.** Cu<sup>2+</sup> in aqueous solution may be theoretically treated as a tetra-coordinated, square planar species [Cu(H<sub>2</sub>O)<sub>4</sub>]<sup>2+</sup> (denoted as Cu<sup>2+</sup> next).<sup>29</sup> From the point of view of coordination chemistry, the interaction of Cu<sup>2+</sup> with A $\beta$  is the process where the coordinated water molecules of Cu<sup>2+</sup> are successively substituted by the atoms of A $\beta$ . Because A $\beta$  is a multidentate ligand and its conformation is highly flexible, the substitution process is unusually intricate. The knowledge about atoms of A $\beta$  and how stepwise substituting the coordinated water molecules of Cu<sup>2+</sup> have been modest up to now. Here, we propose a new strategy to evaluate the coordination priority of atoms of A $\beta$  with Cu<sup>2+</sup> and to explore the coordination mode of Cu<sup>2+</sup>-A $\beta$  complexes based on MD simulations and RDF analyses.

A radial distribution function (RDF),  $g_{ab}(r)$ , describes the probability of finding an atom of type b at a distance between  $r$  and  $r + \Delta r$  from atoms of type a as a function of the a-b separation  $r$ .<sup>30</sup> RDF has been widely used to study the dynamical structural modification of dense systems, the dynamical properties of metal ion hydration, and to search metal binding sites in proteins during MD simulations.<sup>31-34</sup> In current work, the MD data of Cu<sup>2+</sup>-A $\beta$  complexes were processed by RDF analysis, in which Cu<sup>2+</sup> was assigned as the atom of type a and each potential coordination atom of A $\beta$  was assigned as the atom of type b. Three types of data (i.e.,  $[g(r)]_p$ ,  $R_p$ , and  $\Delta r$ ) were extracted from the RDF analysis (Figure 2): (i)  $[g(r)]_p$  denotes the peak value of  $g(r)$  in RDF calculations for one coordinated/potential coordination atom of A $\beta$  with Cu<sup>2+</sup>, which indicates the highest probability of this atom presenting at one certain distance ( $R_p$ ) away from Cu<sup>2+</sup>. (ii)  $R_p$  denotes the value of distance from one coordinated/potential coordination atom of A $\beta$  to Cu<sup>2+</sup>, where the highest probability ( $[g(r)]_p$ ) of this atom presenting away from Cu<sup>2+</sup> is obtained. Therefore, it would be reasonable to consider  $[g(r)]_p$  and  $R_p$  as a pair of conjugate values, both of them describing two of the main characteristics of the peak of  $g(r)$ , that is, how and where the highest peak is. (iii)  $\Delta r$  is defined by the equation  $\Delta r = r_{\max} - r_{\min}$ , where  $r_{\max}$  is the maximum  $r$  value and  $r_{\min}$  is the minimum  $r$  value, with the  $g(r)$  value being zero, respectively;  $r_{\max}$  indicates the maximum distance and  $r_{\min}$  indicates the minimum distance of one coordinated/potential coordination atom of A $\beta$  away from Cu<sup>2+</sup>, respectively.  $\Delta r$ , the difference between  $r_{\max}$  and  $r_{\min}$ , indicates the range of the atom of A $\beta$  away from Cu<sup>2+</sup>. Briefly, these data characterize the distance distribution from the potential coordination atoms of A $\beta$  to Cu<sup>2+</sup> and provide probability information of the potential coordination atoms approaching or in the metal coordination shell.

For rationally evaluating the probability of the potential coordination atoms entering the metal coordination shell and the coordination priority, a novel evaluating function  $Q$  was proposed (eq 1)

$$Q = \frac{R_o}{R_p \log_{10}(\Delta r/r_o)} [10g(r)_p] \quad (1)$$

where  $r_o$  represents the unit length,  $r_o = 1 \text{ \AA}$ , which makes the  $Q$  value a dimensionless quantity, coordination probability.  $R_o$  represents the average bond length of Cu-N/O bonds and is assigned 2.0  $\text{\AA}$ .

Equation 1 integrates the three characteristic quantities,  $[g(r)]_p$ ,  $R_p$ , and  $\Delta r$ , into one formula to reflect the coordination substitutions and fit the coordination probability of Cu<sup>2+</sup> with A $\beta$ . The  $Q$  values of the potential/non-coordinated atoms are

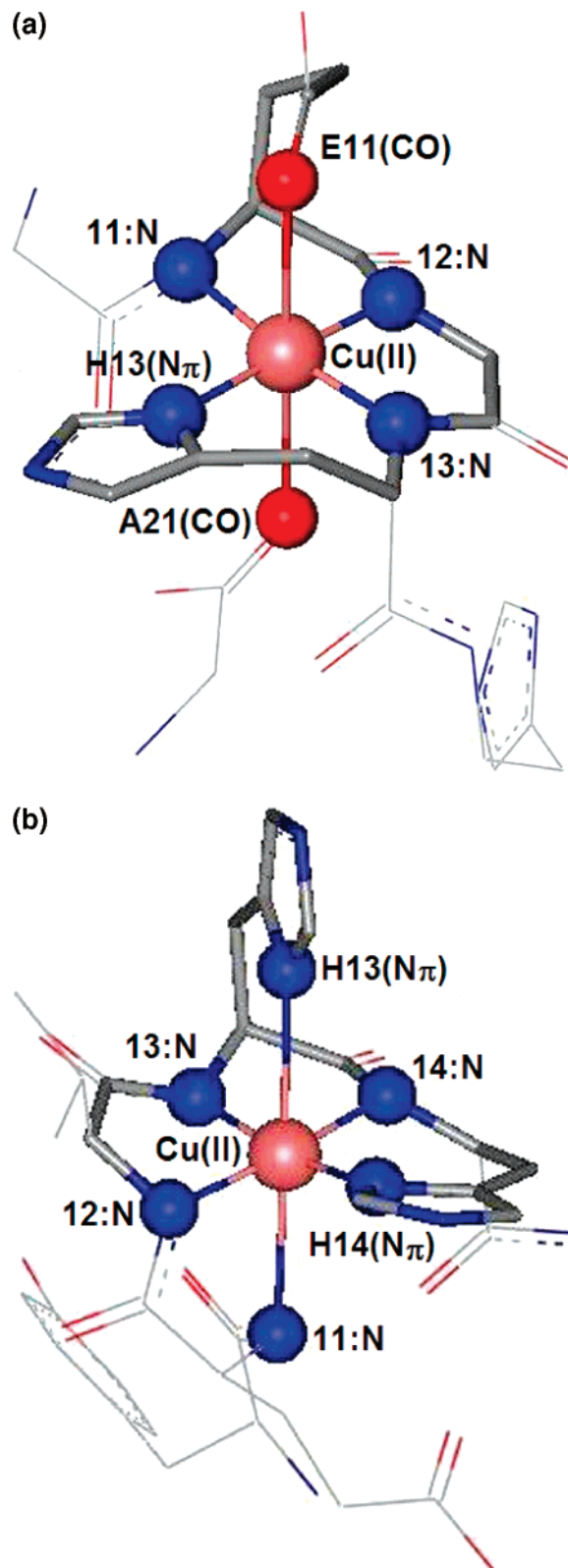


**Figure 4.** Coordination environment of [Cu<sup>2+</sup>-A $\beta$ ] complex (a) in [6-5-5]<sup>1</sup> binding mode and (b) in [6-5-5]<sup>2</sup> binding mode.

always less than 1. By sequencing the corresponding  $Q$  values of the potential coordination atoms in magnitude order, and according to the assumption that the bigger the  $Q$  value is, the higher the coordination probability is, the atom with the coordination priority for each coordination substitute step is filtered. The procedure of evaluating the coordination priority was divided into two steps. First, the RDF analysis of the MD

**TABLE 3.** RDF Evaluation of Coordination Priority of Atoms in Third Substituted  $[\text{Cu}^{2+}\text{-A}\beta]$  Complex

potential coordination atoms	RDF analysis <sup>a</sup>						$Q'$ value <sup>b</sup>	order of coordination priority
	$[g(r)]_p$	$R_p$	$r_{\min}$	$r_{\max}$	$\Delta r$	$Q$ value		
10:N	0.00330	8.0	5.2	8.8	3.6	0.01483	0.88779 1.05703	10
11:N	0.02174	2.8	2.6	4.5	1.9	0.55707		1
12:N	0.25389	1.9	1.8	2.0	0.2			
13:N	0.30229	1.9	1.8	2.0	0.2			
14:N	0.01900	2.9	2.4	4.2	1.8	0.51331	0.99701	2
15:N	0.00719	4.4	3.6	7.2	3.6	0.05875		4
16:N	0.00273	6.2	4.7	10.0	5.3	0.01216		12
17:N	0.00192	8.3	4.8	12.5	7.7	0.00522		17
18:N	0.00165	8.2	5.5	13.4	7.9	0.00448		19
19:N	0.00333	6.6	5.1	11.7	6.6	0.01231		11
20:N	0.00440	6.0	4.6	10.4	5.8	0.01921		9
21:N	0.00218	7.0	4.8	11.2	6.4	0.00773		14
Y10(OH)	0.00193	8.0	4.2	13.6	9.4	0.00496		18
E11(CO)	0.00267	7.1	3.3	9.0	5.7	0.00995		13
E11(OH)	0.00169	8.0	4.3	9.0	4.7	0.00629		15
H13(N $\pi$ )	0.30013	2.0	1.9	2.1	0.2		0.99701	
H13(N $\tau$ )	0.04551	4.1	3.9	4.4	0.5	0.03176		7
H14(N $\pi$ )	0.01359	3.6	2.8	5.8	3.0	0.15824		3
H14(N $\tau$ )	0.00604	5.2	3.0	7.7	4.7	0.03456		6
Q15(N)	0.00540	5.6	4.0	10.4	6.4	0.02392		8
Q15(O)	0.00837	4.2	3.1	10.3	7.2	0.04649		5
K16(N)	0.00047	9.7	7.4	16.1	8.7	0.00103		21
A21(CO)	0.00138	7.0	4.1	12.4	8.3	0.00429		20
A21(OH)	0.00193	7.5	2.9	12.5	9.6	0.00524		16

<sup>a</sup> On the basis of the conformational space consisting of one million conformers. <sup>b</sup>  $Q'$  values of coordinated atoms.

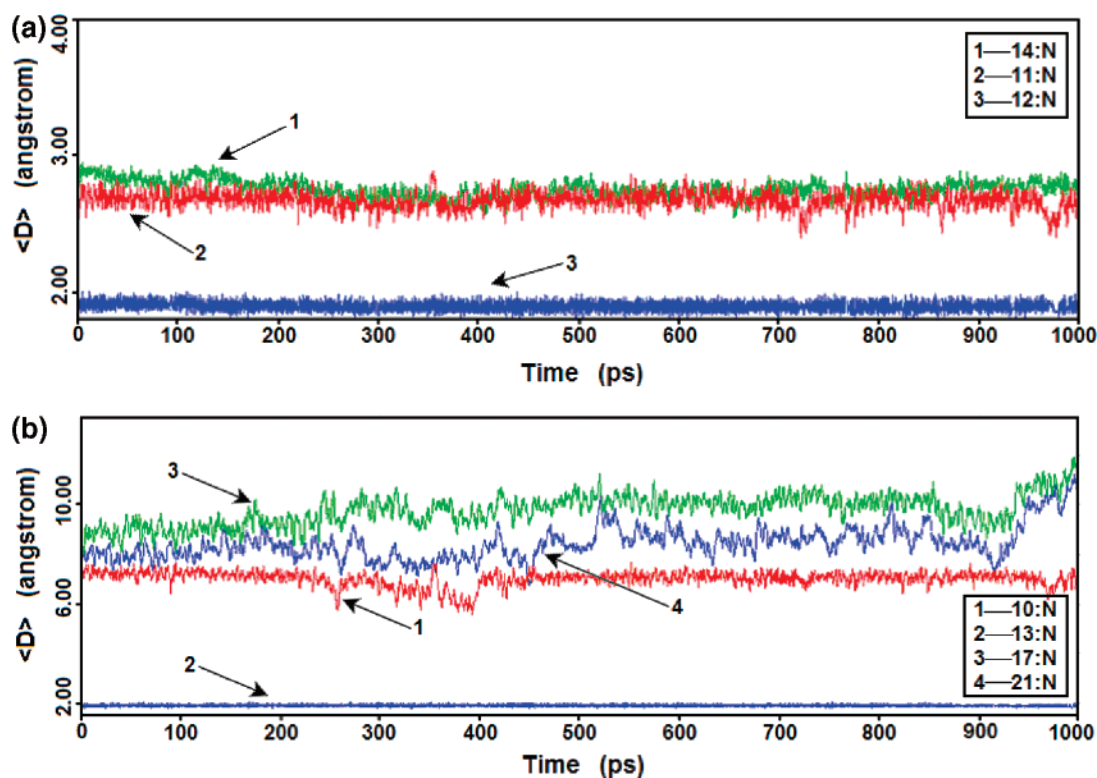


**Figure 5.** Trajectory plots of the distance between  $\text{Cu}^{2+}$  and backbone N atoms in the third substituted  $[\text{Cu}^{2+}\text{-A}\beta]$  complex. (a) Plots of the 11:N, 12:N, and 14:N atoms of the backbone. (b) Plots of the 10:N, 13:N, 17:N, and 21:N atoms of the backbone.

data of each potential coordination atom was performed, and the values of  $[g(r)]_p$ ,  $R_p$ , and  $\Delta r$  for calculating the  $Q$  value were obtained. Second, the potential coordination atoms were sequenced by their  $Q$  values, and the atom with the largest  $Q$  value was selected as the coordination atom for the coordination substitution.

Growing evidence suggests that the histidine residues of  $\text{A}\beta$  are the key binding sites for metal ions. Rat  $\text{A}\beta$ , containing three amino acid substitutions R5G, Y10F, and H13R, binds metal ions much less avidly than human  $\text{A}\beta$ .<sup>11</sup> The ability of

metal ions to aggregate human  $\text{A}\beta$  is diminished by modifying the histidine residues with diethyl pyrocarbonate.<sup>12</sup> The reduced affinity of rat  $\text{A}\beta$  for metal ions is reproduced by the single H13R mutation of human  $\text{A}\beta$ .<sup>35</sup> The atoms, H13(N $\pi$ ), H13(N $\tau$ ), H14(N $\pi$ ), and H14(N $\tau$ ) of  $\text{A}\beta$  (see Figure 3), were assigned as the anchor sites for first substituting one of the coordinated water molecules of  $\text{Cu}^{2+}$  and the initial structures of the first substituted  $\text{Cu}^{2+}\text{-A}\beta$  complexes constructed, respectively. Then MD simulations were performed to search the conformational space of the first substituted  $\text{Cu}^{2+}\text{-A}\beta$  com-

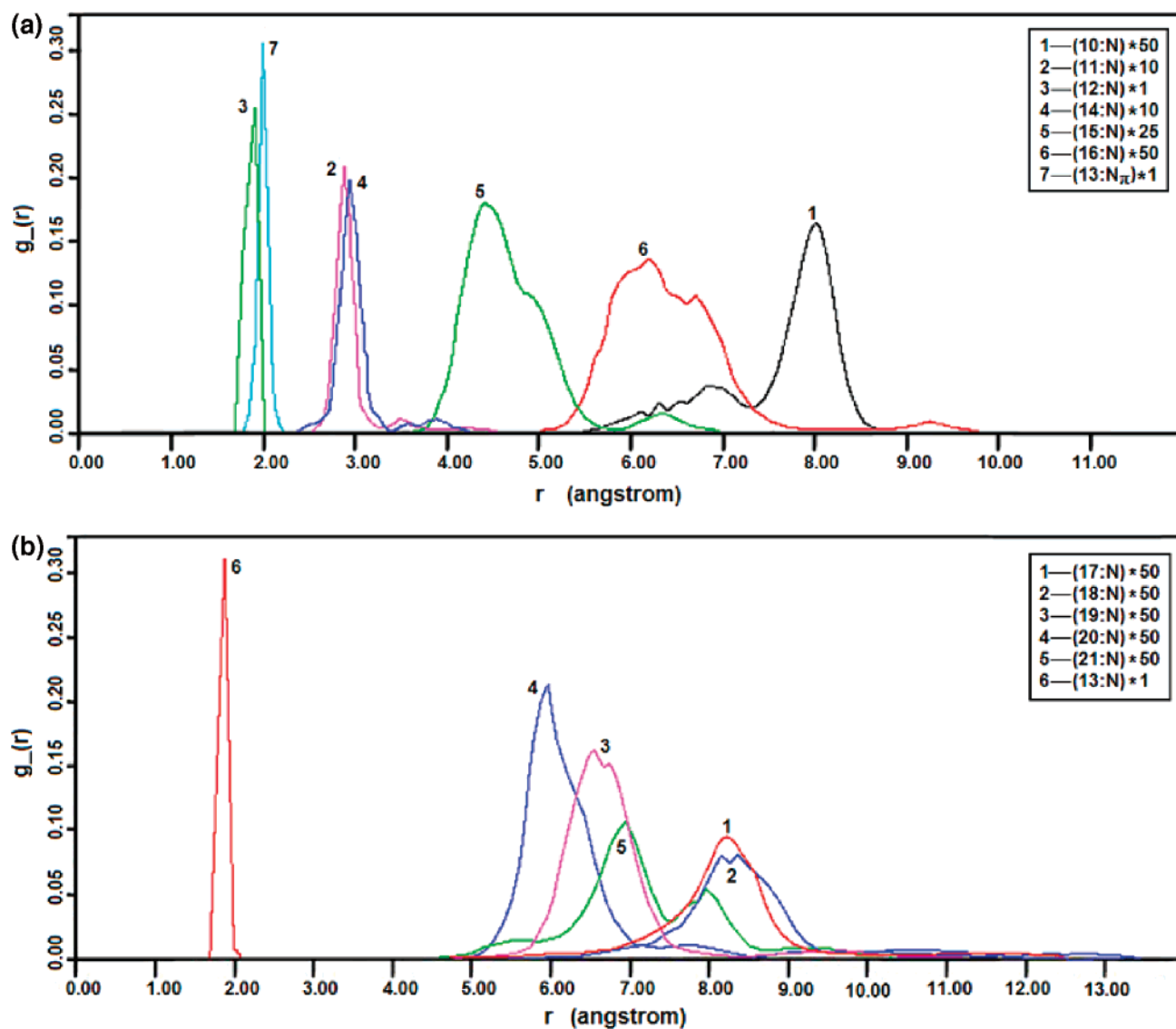


**Figure 6.** RDF plots of the potential coordination atoms in the third substituted  $[\text{Cu}^{2+}\text{-A}\beta]$  complex. (a) RDF plots of the backbone N atoms of the hydrophilic segment with H13(N $\pi$ ) as an inner mark. (b) RDF plots of the backbone N atoms of the hydrophobic segment with (13:N) as an inner mark. Note: (10:N)\*50 in Figure 4a represents that the  $g(r)$  value of the (10:N) atom is magnified 50-fold for clarity. The others are on the analogy of it.

plexes, and the MD data were analyzed by RDF and the  $Q$  function to evaluate the coordination priority of atoms and select the second coordination atom for the second substitution. Using the selected atom substituting one of the coordinated water molecules of the structural optimized  $[\text{Cu}(\text{H}_2\text{O})_3]^{2+}\text{-A}\beta$  complex (i.e., the first substituted complex), the initial structure of the second substituted complex,  $[\text{Cu}(\text{H}_2\text{O})_2]^{2+}\text{-A}\beta$ , was obtained. Repeating the process of the MD conformational search and RDF analysis, the priority coordination atoms for higher substitution (third and fourth) were stepwise obtained.

The first substituted  $\text{Cu}^{2+}\text{-A}\beta$  complexes with all four possible anchor sites, that is, H13(N $\pi$ ), H13(N $\tau$ ), H14(N $\pi$ ), and H14(N $\tau$ ), were calculated, respectively. By using the stepwise substitution scheme mentioned previously, the four fourth substituted  $\text{Cu}^{2+}\text{-A}\beta$  complexes were obtained from the four first substituted  $\text{Cu}^{2+}\text{-A}\beta$  complexes (Supporting Information Tables S1–S3). The corresponding optimization conformations of the four fourth substituted  $\text{Cu}^{2+}\text{-A}\beta$  complexes were obtained by the structural optimization procedure discussed next, among which the complex with H13(N $\pi$ ) as the anchor site (represented as the  $[\text{Cu}^{2+}\text{-A}\beta]$  complex) is the stablest one (Table 1). So, we focused our attention on this species.

The procedure combining molecular dynamics and energy minimization was carried out for structural optimizations of the  $\text{Cu}^{2+}\text{-A}\beta$  complexes of any substitution degree. (i) The initial conformation of the substituted  $\text{Cu}^{2+}\text{-A}\beta$  complex was first equilibrated by running dynamics of 1 ns. A total of 10 000 conformations was sampled at 100 fs intervals during a subsequent 1 ns stage for data collection. (ii) By averaging the 10 000 conformations, a dynamic average conformation was extracted. (iii) Submitting the dynamic average conformation to energy minimization: first by the steepest descent method, followed by the conjugate gradient method, until the rms derivative fell below  $0.1 \text{ kcal mol}^{-1} \text{ \AA}^{-1}$ , the structurally optimized complex was obtained. It should be noted that the optimized average structures obtained from the previous procedure are different from the optimized structures from extensive conformational searches. However, the optimized average structure might be a rational approximation to the optimized structures from conformational searches. As the template effect of Cu(II) on the conformation of A $\beta$  makes the local structure of the peptide rigidize, which results in the limited entropy of the  $\text{Cu}^{2+}\text{-A}\beta$  complexes, there is a large chance that the average

structures might be close to the real optimized structures, especially for the highly coordinated  $\text{Cu}^{2+}$ - $A\beta$  complexes.

Table 2 shows the priority coordination atoms of each substitution step of the  $[\text{Cu}^{2+}$ - $A\beta$ ] complex. Meanwhile, the [6-5-5] coordination mode of the  $[\text{Cu}^{2+}$ - $A\beta$ ] complex was obtained, that is, H13( $N\pi$ ) and its adjacent backbone N atoms, 11:N, 12:N, and 13:N, acted as the essential coordination sites, forming the equatorial plane with a 6-membered ring/5-membered ring/5-membered ring, and the side chain atoms, E11-(CO) and A21(CO), axially coordinated (Figure 4a). The axial coordination was characterized by the smaller  $Q'$  values, 0.42814 and 0.42160, and the longer distance from  $\text{Cu}^{2+}$ , 2.6 Å, which may be connected to the Jahn–Teller effect.

During the process of evaluating the coordination priority, we found an interesting phenomenon for the third substituted  $[\text{Cu}^{2+}$ - $A\beta$ ] complex. Table 3 shows the order of coordination priority of the atoms for the third substituted  $[\text{Cu}^{2+}$ - $A\beta$ ] complex. The  $Q$  values of 11:N and 14:N are 0.55707 and 0.51331, respectively, which are less than 1, yet larger than the  $Q$  values of the other non-coordinated atoms. According to the  $Q$  value, 11:N was screened as the binding site for the fourth substitution. The  $Q$  value of 11:N, however, is close to that of 14:N, which suggests that there may exist a coordination competition between them. Maybe just because of the competition of 14:N, the  $Q$  value of 11:N (0.55707) is markedly less than that of the priority atoms of the first (0.87930) and the second (0.92590) substitution (Table 2).

Taking 14:N as the fourth substitution atom, we carried out the further MD simulations, RDF analyses, and  $Q$  function evaluations and found another possible coordination environment of the [6-5-5] coordination mode (represented as the  $[6-5-5]^2$  mode next). H14( $N\pi$ ) and its adjacent backbone N atoms, 12:N, 13:N, and 14:N, form the equatorial plane with a 6-membered ring/5-membered ring/5-membered/ring, and the side chain atom H13( $N\pi$ ) and the backbone atom 11:N axially coordinate  $\text{Cu}^{2+}$  (Figure 4b and Supporting Information Table S4). The optimized energy ( $-372.8699$  kJ/mol) of the  $[\text{Cu}^{2+}$ - $A\beta$ ] complex with the  $[6-5-5]^2$  mode is a little higher than that ( $-418.9749$  kJ/mol) of the  $[\text{Cu}^{2+}$ - $A\beta$ ] complex with the  $[6-5-5]^1$  mode. The previous two coordination modes may coexist with each other. Both of them are characterized by forming the equatorial plane with the 6-membered ring/5-membered ring/5-membered ring consisting of one histidine imidazole  $N\pi$  atom and its adjacent backbone N atoms. This intramolecular coordination mode is consistent with experimental results.<sup>13,37</sup>

Figure 5a shows that the trajectory of the 12:N atom fluctuates near the axis apart from  $\text{Cu}^{2+}$  by approximately 1.9 Å, indicating that it is in a coordinated state with  $\text{Cu}^{2+}$ . As compared with other non-coordinated atoms (see Figure 5b and Supporting Information Figure S2a,b), the trajectories of 11:N and 14:N fluctuate near the axis apart from  $\text{Cu}^{2+}$  by approximately 2.8 Å, which is the nearest distance of the potential coordination atoms to  $\text{Cu}^{2+}$ . Meanwhile, the trajectories of 11:N and 14:N are almost superimposed, indicating that their coordination priorities may be close to each other and that they may be mutually competitive coordination atoms. This result is consistent with that of the  $Q$  function analyses (Table 3 and Figure 6).

**3.2.  $\text{Cu}^{2+}$ -Induced Conformational Transition of  $A\beta$ .**  $A\beta$  is a typical amphiphilic molecule with a hydrophilic N-terminal and hydrophobic C-terminal (Figure 7a). Taking the initial  $\beta$  conformation  $A\beta$  as the conformational reference, the conformational transition of the dynamic average conformations of the

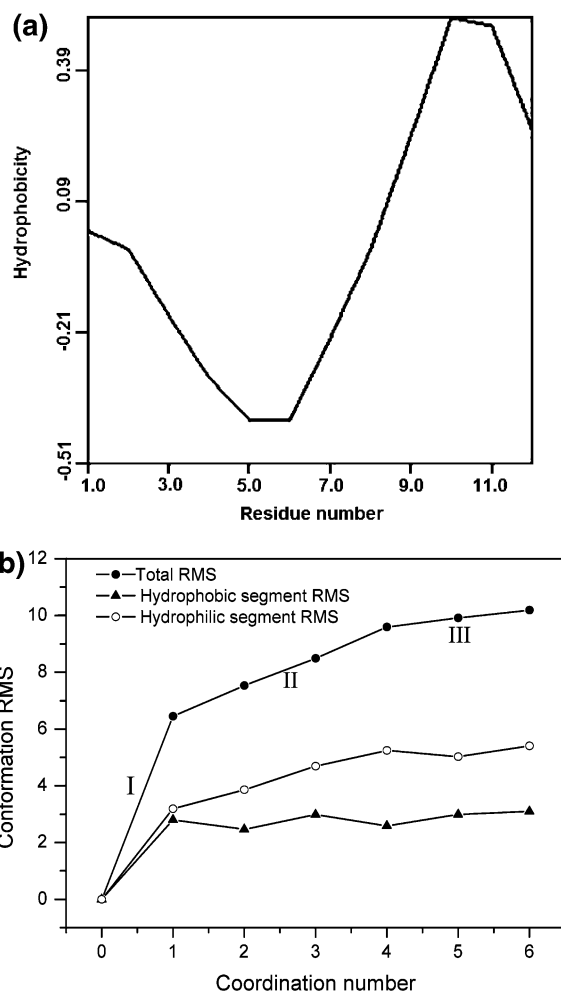


**Figure 7.** (a) Hydrophobic property of  $A\beta$  by the Eisenberg–Weiss scheme.<sup>30</sup> (b) rms analysis of the conformational transition of  $[\text{Cu}^{2+}$ - $A\beta$ ] complexes with substituted degrees from one to six.

$[\text{Cu}^{2+}$ - $A\beta$ ] complexes with different substituted degrees was analyzed by the rms method, which is based on calculating a minimum rms value (Supporting Information eq S1) from superimposing the corresponding atoms selected from two molecules.<sup>30</sup> Here, 12 pairs of corresponding backbone  $\alpha$  carbon atoms from the initial  $\beta$  conformation  $A\beta$  and every  $[\text{Cu}^{2+}$ - $A\beta$ ] complex with a certain substituted degree were used to perform a minimum rms calculation. The trend of the conformational transition of the hydrophobic segment  $L_{17}$ VFFA<sub>21</sub> is significantly different from that of the hydrophilic segment  $Y_{10}$ -EVHHQK<sub>16</sub> (Figure 7b). The conformational transition trend of the hydrophobic segment can be divided into two parts: (i) a sharp conformational transition of the first substituted complex and (ii) a mild fluctuation of the conformational transition of the complexes with a substitution number from two to six. For the hydrophilic segment, the trend can be divided into three parts: (i) a marked conformational transition of the first substituted complex; (ii) a gradual conformational transition of the complexes with substitution numbers from two to four; and (iii) a slight conformational transition of complexes with substitution numbers from four to six. Particularly, the trend of the conformational transition of total  $A\beta$  is nearly parallel to that of the hydrophilic segment from the first substitution to the sixth.

The detailed conformation analysis indicated that the coordinated water molecules of  $\text{Cu}^{2+}$  directly formed several hydrogen bonds with  $A\beta$  and induced it, forming more intramo-

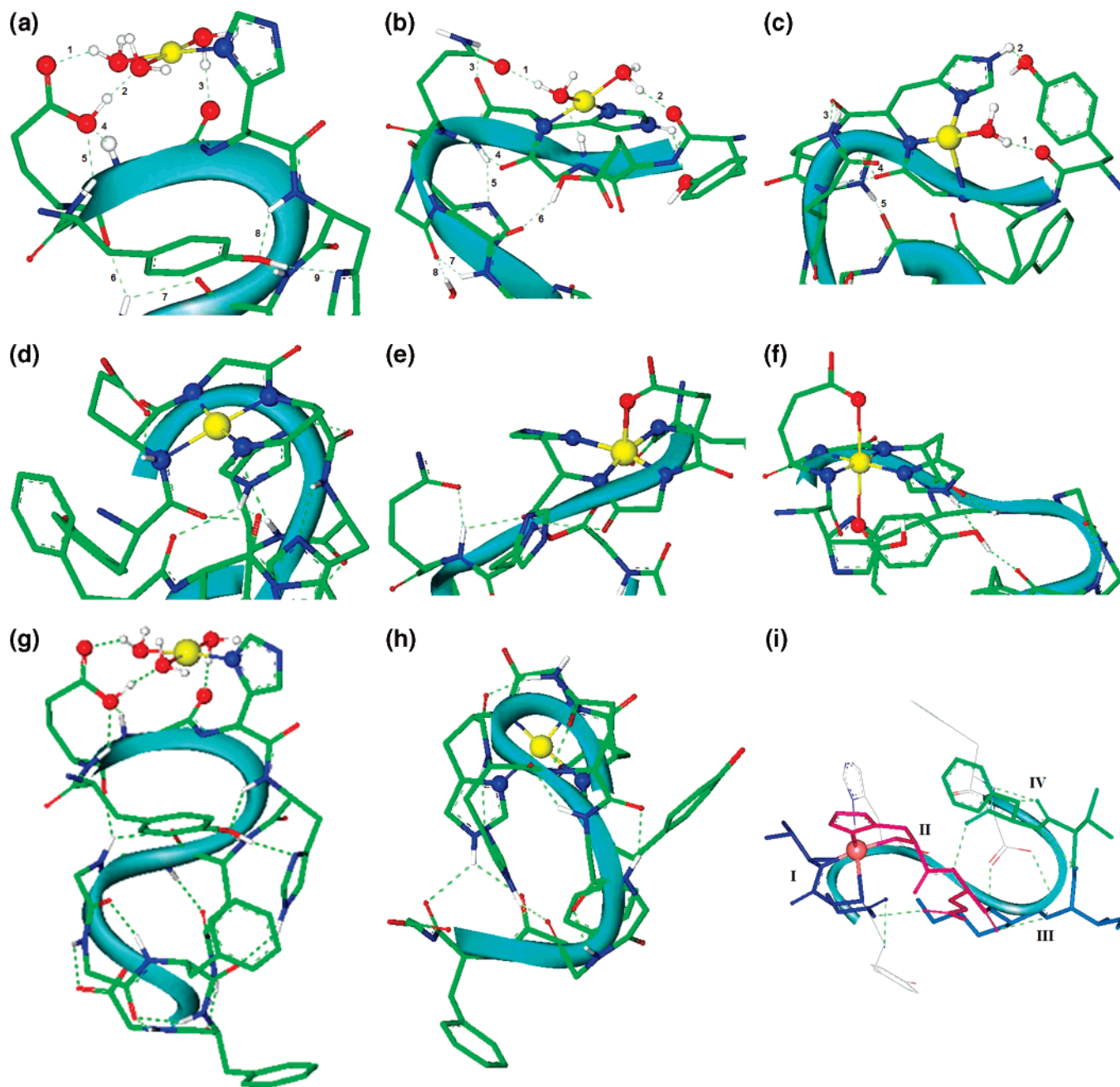


**Figure 8.** Possible driving force for the conformational transition of  $[\text{Cu}^{2+}\text{-A}\beta]$  complexes. Water-bridged coordination bonds and hydrogen bond network (a) in the first substituted complex, (b) in the second substituted complex, and (c) in the third substituted complex. Coordination bonds and hydrogen bond network (d) in the fourth substituted complex, (e) in the fifth substituted complex, and (f) in the sixth substituted complex. (g) Water-bridged coordination bonds and hydrogen bond network in the first substituted complex. (h) Coordination bonds and hydrogen bond network in the fourth substituted complex. (i) Conformation of the  $[\text{Cu}^{2+}\text{-A}\beta]$  complex in  $[6\text{-}5\text{-}5]^2$  binding mode. Regions I and II form loop I, driven mainly by the cooperation of coordination bonds and hydrogen bonds. Regions III and IV form loop II, driven mainly by hydrogen bonds. The conformation parameters are shown in Table 4.

lecular hydrogen bonds. The coordinated water molecules of  $\text{Cu}^{2+}$  bridged the coordination bonds and the hydrogen bonds as a network, which may result in the sharp conformational transition of the first substituted complex (Figure 8a,g). With the increase of the substituted degree, the number of coordination bonds between  $\text{Cu}^{2+}$  and A $\beta$  increased, yet the number of water-bridged hydrogen bonds decreased for the decrease of the coordinated water molecules. The coordination bonds may gradually become the main force that drives the conformational transition of the hydrophilic segment (Figure 8b–d,h). Because the strength of one coordination bond is approximately 10-fold as much as that of one hydrogen bond, the increased coordination bonds not only counteract the negative influence from the

decrease of the hydrogen bonds but also continuously drive the conformational transition of the hydrophilic segment in a gentle manner. As the coordination interaction in an axial direction is usually weaker (the Jahn–Teller effect), the fifth and sixth coordination just bring about a slight conformational transition (Figure 8e,f).

From the first substitution, the intramolecular hydrogen bond network has formed (Figure 8g) and drives the hydrophobic segment, almost finishing its conformational transition. As the influence of the coordination interaction of  $\text{Cu}^{2+}$  to the hydrophobic segment is indirect, the conformation of the hydrophobic segment just fluctuates with the increase of the substitution degree. After the first substitution, a markedly

**TABLE 4. Conformation Parameters of Cu<sup>2+</sup>-A $\beta$  Complex in [6-5-5]<sup>2</sup> Binding Mode**

conformation features		loop I					loop II				
residues		E11	V12	H13	H14	Q15	K16	L17	V18	F19	F20
dihedral	F	-66.7	-103.7	177.0	-52.1	92.2	-72.2	58.4	-76.2	27.3	-71.9
	Y	-41.6	-9.3	-43.5	131.6	8.7	74.2	-56.4	54.3	-63.4	-39.5

**TABLE 5. Comparison of Stability of Aggregating Systems (kJ/mol)<sup>a</sup>**

strands number	energy of initial structure	energy of [6-5-5] <sup>1</sup> complex	increased energy of [6-5-5] <sup>1</sup> complex
4	-192.3242	+42.3463	+234.6705
16	-1281.7756	+252.2744	+1534.0500

<sup>a</sup> Potential of the single strand A $\beta$  of the initial structure and that of the [6-5-5]<sup>1</sup> complex were regarded as reference values, respectively.

**TABLE 6. Comparison of Stability of Aggregating Systems (kJ/mol)<sup>a</sup>**

strands number	energy of initial structure	energy of [6-5-5] <sup>2</sup> complex	increased energy of [6-5-5] <sup>2</sup> complex
4	-192.3242	+35.1436	+227.4678
16	-1281.7756	+218.8632	+1500.6388

<sup>a</sup> Potential of the single strand A $\beta$  of the initial structure and that of the [6-5-5]<sup>2</sup> complex were regarded as reference values, respectively.

conformational transition occurs to both the hydrophilic segment and the hydrophobic one, so the curve of part I is very sharp (Figure 7b). The conformational transition curve of A $\beta$  is nearly parallel to that of the hydrophilic segment, which indicates that the conformational transition of A $\beta$  may be determined mainly by the hydrophilic segment.

Figure 8i and Table 4 show that driven by the cooperation of six coordination bonds and 10 hydrogen bonds, the conformation of A $\beta$  transforms from a  $\beta$  conformation type to a distorted  $\beta$  one, such as the loop conformation.

**3.3. Comparative Study of the Stability of Aggregating Systems.** Using the three kinds of monomers (i.e., the [Cu<sup>2+</sup>-A $\beta$ ] complex of [6-5-5]<sup>1</sup> mode, the [Cu<sup>2+</sup>-A $\beta$ ] complex of [6-5-5]<sup>2</sup> mode, and the initial  $\beta$  conformation A $\beta$ ), two types of fibrils consisting of four and 16 monomers were assembled according to the parameters of the fibril model (Figure 1), respectively.

Tables 5 and 6 show the results of the structural optimization of the six kinds of aggregating systems. The energy trend of the fibrils consisting of the initial A $\beta$  and [Cu<sup>2+</sup>-A $\beta$ ] complexes (distorted A $\beta$ ) are oppositional with the increase of monomer numbers, that is, the energy of fibrils consisting of the initial A $\beta$  becomes lower, yet the energy of fibrils consisting of distorted A $\beta$  becomes higher. The energy difference between fibrils consisting of the initial A $\beta$  and those consisting of the [Cu<sup>2+</sup>-A $\beta$ ] complex of the [6-5-5]<sup>1</sup> mode is from 234.6705 to 1534.0500 kJ/mol with monomer numbers from four to 16. Similarly, the energy difference between fibrils consisting of the initial A $\beta$  and those consisting of the [Cu<sup>2+</sup>-A $\beta$ ] complex of the [6-5-5]<sup>2</sup> binding mode is from 227.4678 to 1500.6388 kJ/mol with monomer numbers from four to 16. The previous data indicate that the stability of the aggregating systems assembled by the [Cu<sup>2+</sup>-A $\beta$ ] complexes (distorted A $\beta$ ) is far lower than that of the fibrils assembled by the  $\beta$  conformation monomer.

#### 4. Conclusion

On the basis of the principles of coordination chemistry, the coordination mode of the [Cu<sup>2+</sup>-A $\beta$ ] complexes under neutral

pH was investigated for the first time by MD simulations. On the basis of the RDF analysis of the conformational space of the [Cu<sup>2+</sup>-A $\beta$ ] complexes, we proposed a new strategy, the *Q* function, to evaluate the coordination priority of potential atoms of A $\beta$  in the process of coordination substitution. The [6-5-5] tri-ring 4N coordination mode of the Cu<sup>2+</sup>-A $\beta$  complexes was found (i.e., the histidine N $\pi$  atom acting as the anchor site and its adjacent backbone N atoms as the essential coordination sites form the equatorial plane with a 6-membered ring/5-membered ring/5-membered-ring). This result is consistent with Miura et al.'s experimental data<sup>13</sup> and the fact that Cu<sup>2+</sup> may promote the ionization of amide groups of a peptide if a histidine residue is available as a primary binding site.<sup>36,38</sup>

It has been revealed that the  $\beta$  conformation of A $\beta$  is not only the most preferential form for aggregation but also the structural basis of the assembling forces, such as hydrogen bonds, van der Waals interactions, and hydrophobic interactions (Figure 1).<sup>15,19,25</sup> Once the  $\beta$  conformation of A $\beta$  is severely distorted, the conditions for forming hydrogen bonds between the main chains will disappear, and van der Waals and hydrophobic interactions will be weakened by the disorder of the stretching directions of the side chains, which may make A $\beta$  lose its assembling forces and exist in a soluble form in solutions.<sup>15</sup> Driven by the cooperation of coordination bonds and hydrogen bonds, the coordination of Cu<sup>2+</sup> with A $\beta$  under the [6-5-5] mode makes the conformation of A $\beta$  transform from a  $\beta$  conformation to a distorted  $\beta$  type. Thus, two histidines of different peptide chains in the folded distorted  $\beta$  conformation would not be able to approach each other to form an intermolecular His(N $\pi$ )-metal-His(N $\pi$ ) bridge. The stability study of the fibrils indicates that the monomers with the distorted  $\beta$  conformation make the stability of the aggregating systems assembled by them dramatically decrease. The Cu<sup>2+</sup>-A $\beta$  complexes go against forming stable fibrils and Cu<sup>2+</sup> inhibits A $\beta$  from aggregating into fibrils.

The coordination mode of Cu<sup>2+</sup> with some important proteins, such as prion protein (PrP) and A $\beta$ , is characterized by soluble chelation.<sup>13,37,39-42</sup> Cu<sup>2+</sup> forms soluble complexes with the octapeptide repeat (PHGGGWGQ)*n*, which occurs near the N-terminus of the prion protein and has a high affinity for Cu<sup>2+</sup>. In the Cu<sup>2+</sup>-(PHGGGWGQ)*n* complex, the histidine N $\pi$  atom together with deprotonated amide nitrogens act as ligands.<sup>39</sup> Cu<sup>2+</sup> pronouncedly inhibits the conversion of full-length recombinant PrP (rPrP 23-230) into amyloid fibrils, and other metal ions have less or no effect on the conversion.<sup>42</sup> Cu<sup>2+</sup> of physiological concentrations can critically alter the stability of the toxic A $\beta$  oligomers and can potentially control the course of neurodegeneration.<sup>41</sup> The study of the mechanism of Cu<sup>2+</sup>-A $\beta$  interactions is significant in improving the understanding of the pathology of neurodegenerative diseases and in contributing to the development of an anti-amyloid therapeutic strategy.<sup>43,44</sup>

**Acknowledgment.** The authors thank the reviewers for their comments. This work is supported by the National Natural Science Foundation of China (Grants 30470408 and 20637010) and the Youth Scientific and Technical Research Foundation of Shanxi Province (Grant 2006021009).

**Supporting Information Available:** Data of RDF evaluation of coordination priority of atoms in Cu<sup>2+</sup>-A $\beta$  complexes with H13(N $\tau$ ), H14(N $\pi$ ), and H14(N $\tau$ ) as anchor sites, respectively (Tables S1–S3). Data of RDF evaluation of coordination priority of atoms in [6-5-5]<sup>2</sup> binding mode (Table S4). RDF plots of potential coordination atoms of side chain in third substituted [Cu<sup>2+</sup>-A $\beta$ ] complex (Figure S1). Trajectory plots of distance between Cu<sup>2+</sup> and backbone N atoms in third substituted [Cu<sup>2+</sup>-A $\beta$ ] complex (Figure S2). Formula for calculating  $Q'$  values of coordinated atoms (eq S1). Formula for rms calculations (eq S2). This material is available free of charge via the Internet at <http://pubs.acs.org>.

## References and Notes

- (1) Selkoe, D. J. *Neuron* **1991**, *6*, 487–498.
- (2) Leslie, R. A. *Trends Neurosci.* **2002**, *25*, 232–233.
- (3) Glenner, G. G.; Wong, C. W. *Biochem. Biophys. Res. Commun.* **1984**, *120*, 885–890.
- (4) Masters, C. L.; Simms, G.; Weinman, N. A.; Multhaup, G.; McDonald, B. L.; Beyreuther, K. *Proc. Natl. Acad. Sci. U.S.A.* **1985**, *82*, 4245–4249.
- (5) Kang, J.; Lemaire, H. G.; Unterbeck, A.; Salbaum, J. M.; Masters, C. L.; Grzeschik, K. H.; Multhaup, G.; Beyreuther, K.; Muller-Hill, B. *Nature* **1987**, *325*, 733–736.
- (6) Selkoe, D. J. *Physiol. Rev.* **2001**, *81*, 741–766.
- (7) Lovell, M. A.; Robertson, J. D.; Teesdale, W. J.; Campbell, J. L.; Markesbery, W. R. *J. Neurol. Sci.* **1998**, *158*, 47–52.
- (8) Liu, G. J.; Huang, W. D.; Moir, R. D.; Vanderburg, C. R.; Lai, B.; Peng, Z. C.; Tanzi, R. E.; Rogers, J. T.; Huang, X. D. *J. Struct. Biol.* **2006**, *155*, 45–51.
- (9) Frederickson, C. J.; Bush, A. I. *Biometals* **2001**, *14*, 353–366.
- (10) Bush, A. I.; Pettingell, W. H.; Multhaup, G.; Paradis, M. D.; Vonsattel, J. P.; Gusella, J. F.; Beyreuther, K.; Masters, C. L.; Tanzi, R. E. *Science* **1994**, *265*, 1464–1467.
- (11) Bush, A. I.; Pettingell, W. H.; Paradis, M. D.; Tanzi, R. E. *J. Biol. Chem.* **1994**, *269*, 12152–12158.
- (12) Atwood, C. S.; Moir, R. D.; Huang, X.; Scarpa, R. C.; Bacarra, N. M.; Romano, D. M.; Hartshorn, M. A.; Tanzi, R. E.; Bush, A. I. *J. Biol. Chem.* **1998**, *273*, 12817–12826.
- (13) Miura, T.; Suzuki, K.; Takeuchi, H. *Biochemistry* **2000**, *39*, 7024–7031.
- (14) Suzuki, K.; Miura, T.; Takeuchi, H. *Biochem. Biophys. Res. Commun.* **2001**, *285*, 991–996.
- (15) Zou, J.; Kajita, K.; Sugimoto, N. *Angew. Chem., Int. Ed.*, **2001**, *40*, 2274–2277.
- (16) Deibel, M. A.; Ehmann, W. D.; Markesbery, W. R. *J. Neurol. Sci.* **1996**, *143*, 137–142.
- (17) Zanuy, D.; Nussinov, R. *J. Mol. Biol.* **2003**, *329*, 565–584.
- (18) Hwang, W.; Zhang, S. G.; Kamm, R. D.; Karplus, M. *Proc. Natl. Acad. Sci. U.S.A.* **2004**, *101*, 12916–12921.
- (19) Xu, Y. C.; Shen, J. H.; Luo, X. M.; Zhu, W. L.; Chen, K. X.; Ma, J. P.; Jiang, H. L. *Proc. Natl. Acad. Sci. U.S.A.* **2005**, *102*, 403–5407.
- (20) Straub, J. E.; Guevara, J.; Huo, S. H.; Lee, J. P. *Chem. Res.* **2002**, *35*, 473–481.
- (21) Ma, B. Y.; Nussinov, R. *Proc. Natl. Acad. Sci. U.S.A.* **2002**, *99*, 14126–14131.
- (22) Burkoth, T. S.; Benzinger, T. L. S.; Urban, V.; Morgan, D. M.; Gregory, D. M.; Thiyagarajan, P.; Botto, R. E.; Meredith, S. C.; Lynn, D. G. *J. Am. Chem. Soc.* **2000**, *122*, 7883–7889.
- (23) Han, D. X.; Yang, P. *Sci. China, Ser. B* **2004**, *47*, 126–133.
- (24) Morgan, D. M.; Dong, J.; Lynn, D. G. *J. Am. Chem. Soc.* **2002**, *124*, 12644–12645.
- (25) Petkova, A. T.; Ishii, Y.; Balbach, J. J.; Antzutkin, O. N.; Leapman, R. D.; Delaglio, F.; Tycko, R. *Proc. Natl. Acad. Sci. U.S.A.* **2002**, *99*, 16742–16747.
- (26) Dong, J.; Shokes, J. E.; Scott, R. A.; Lynn, D. G. *J. Am. Chem. Soc.* **2006**, *128*, 3540–3542.
- (27) Zhang, C. F.; Yang, P. *Biochem. Biophys. Res. Commun.* **2006**, *345*, 43–49.
- (28) Shi, S. H.; Yan, L.; Yang, Y.; Fisher-Shaulsky, J.; Thacher, T. J. *Comput. Chem.* **2003**, *24*, 1059–1076.
- (29) Rickard, G. A.; Gomez-Balderas, R.; Brunelle, P.; Raffa, D. F.; Rauk, A. J. *Phys. Chem. A* **2005**, *109*, 8361–8370.
- (30) Accelrys Inc. *Insight II 2000 Program*, release 2000; Accelrys Inc.: San Diego, 2000.
- (31) Yamashita, M. M.; Wesson, L.; Eisenman, G.; Eisenberg, D. *Proc. Natl. Acad. Sci. U.S.A.* **1990**, *87*, 5648–5652.
- (32) Spohr, E.; Palinkas, G.; Heinzinger, K.; Bopp, P.; Probst, M. M. *J. Phys. Chem.* **1988**, *92*, 6754–6761.
- (33) Yang, Z. Z.; Li, X. *J. Phys. Chem. A* **2005**, *109*, 3517–3520.
- (34) Yang, Z. Z.; Li, X. *J. Chem. Phys.* **2005**, *123*, 94507/1–94507/10.
- (35) Liu, S. T.; Howlett, G.; Barrow, C. J. *Biochemistry* **1999**, *38*, 9373–9378.
- (36) Sundberg, R. J.; Martin, R. B. *Chem. Rev.* **1974**, *74*, 471–517.
- (37) Stellato, F.; Menestrina, G.; Serra, M. D.; Potrich, C.; Tomazzolli, R.; Meyer-Klaucke, W.; Morante, S. *Eur. Biophys. J.* **2006**, *35*, 340–351.
- (38) Sigel, H.; Martin, R. B. *Chem. Rev.* **1982**, *82*, 385–426.
- (39) Miura, T.; Hori-i, A.; Mototani, H.; Takeuchi, H. *Biochemistry* **1999**, *38*, 11560–11569.
- (40) Bocharova, O. V.; Breydo, L.; Salnikov, V. V.; Baskakov, I. V. *Biochemistry* **2005**, *44*, 6776–6787.
- (41) Garai, K.; Sengupta, P.; Sahoo, B.; Maiti, S. *Biochem. Biophys. Res. Commun.* **2006**, *345*, 210–215.
- (42) Zong, X. H.; Zhou, P.; Shao, Z. Z.; Chen, S. M.; Chen, X.; Hu, B. W.; Deng, F.; Yao, W. H. *Biochemistry* **2004**, *43*, 11932–11941.
- (43) Bush, A. I. *Curr. Opin. Chem. Biol.* **2000**, *4*, 184–191.
- (44) Bush, A. I. *Trends Neurosci.* **2003**, *26*, 207–214.